ISSN 1810-2328, Journal of Engineering Thermophysics, 2024, Vol. 33, No. 3, pp. 547–565. © Pleiades Publishing, Ltd., 2024.

An Effect of Mass Transpiration and Darcy–Brinkman Model on Ostwald–de Waele Ternary Nanofluid

U. S. Mahabaleshwar[1*], S. M. Sachhin[1], L. M. Pérez[2***], and G. Lorenzini[3****]**

[1]*Department of Studies in Mathematics, Davangere University, Shivagangothri, Davangere, 577 007, India*

[2]*Departamento de Ingeniería Industrial y de Sistemas, Universidad de Tarapacá, Casilla 7D, Arica, Chile*

[3]*Department of Engineering and Architecture, University of Parma, Parma, Italy*

Received November 21, 2023; in final form, June 26, 2024; accepted July 13, 2024

Abstract—This article studies the flow of Ostwald–de Waele ternary nanofluid over a permeable shrinking sheet. The governing partial differential equations are converted into ordinary differential equations using similarity variables and solved analytically. The article includes closed-form algebraic solutions and graphical flow dynamics analysis, dependent on Darcy number, volume fraction, and mass transpiration. The study shows that the presence of porous media significantly upsurges the mass transpiration and magnitude of skin friction. The calculation uses a combination of Titanium dioxide (TiO_2), Cobalt ferrite ($CoFe_2O_4$), and Magnesium oxide (MgO) nanoparticles in pure water, and the ternary nanofluid performs better than the conventional fluid in terms of thermal conductivity. This is important in the fields of manufacturing, machine operations, and engineering, where improving heat transfer is crucial.

DOI: 10.1134/S181023282403010X

HIGHLIGHTS

- Study of Ostwald–de Waele ternary nanofluid over a permeable shrinking surface.
- Momentum equation includes Darcy-Brinkman model.
- Porous media significantly increases the magnitude of skin friction.
- Increasing the volume fraction decreases the velocity profile.
- Governing PDEs are transformed into ODEs via similarity variables.

1. INTRODUCTION

A wide range of areas have paid significant attention to power-law fluids moving in heterogeneous porous surfaces, a natural nonlinear seepage flow phenomenon. The power-law liquids have been the focus of numerous investigations and significant advancements by scientists nowadays. The impact of rheological parameters on a modified drag model for the power-law fluid–particle movement was investigated by Pang et al. [1]. Mahabaleshwar et al. [2] studied the slanting magnetohydrodynamic power-law nanofluid movements caused by a decreasing sheet with mass dissipation. The effects of viscous dissipation, heat radiation, an irregular transverse magnetic field, and non-uniform heat production on the magnetohydrodynamic motion of a power-law fluid with changing fluid characteristics through a nonlinear stretching sheet were examined by Elfeshawey and Waheed [3]. The effect of both a power law liquid and an angled magnetic field on diffusive convection in a lid-driven linear cavity was explored by Hussain and Oztop [4]. With the use of the lattice Boltzmann technique, the inertial migration of elliptical and rectangular particles in a channel movement of a

*E-mail: u.s.m@davangereuniversity.ac.in
**E-mail: sachinsm030@gmail.com
***E-mail: lperez@academicos.uta.cl
****E-mail: giulio.lorenzini@unipr.it

power-law fluid is investigated by Hu et al. [5]. Usman et al. [6] studied the Ostwald–de Waele fluid's heat transfer phenomena in the presence of a heat source/sink within two extensible disks that are coaxially spinning and separated by a uniform distance.

The term porous medium refers to any substance that consists of a solid structure and an interconnected space. Numerous applied science as well as engineering fields make use of the idea of porous media, including purification, mechanics, acoustics, geomechanics, soil mechanics, rock mechanics, physics, biological science, and material science. The effect of changing the field of gravity and movement of tiny fluids' convective instability in a porous medium is investigated numerically using the Galerkin approach by Yadav et al. [7]. Wahid et al. [8] studied the Marangoni hybrid nanofluid movement across an infinite disk that is permeable and embedded in a porous media. Carreau-Yasuda nano liquid including gyrotactic motile microorganisms for its dual conductivity variable over a porous media was numerically studied by Waqas et al. [9]. A porous medium and an inclined nanofluid symmetric channel in the presence of MHD peristaltic transport were examined numerically by Abd-Alla et al. [10]. Eid and Nafe et al. [11] studied the impacts of modifying thermal conductivity and heat production on the movement of magneto-hybrid tiny fluids in porous material under a slip condition. By using a porous media and taking into consideration velocity and thermal slippage, Williamson nanofluid MHD boundary layer motion along a stretched surface influences thermal radiation was studied by Reddy et al. [12].

A fluid called a "nanofluid" is made up of tiny particles dispersed through a base fluid. Less than 100 nm is the usual size of nanoscale particles. The nanofluids were initially put out by Choi and Eastman in 1995. When nanoparticles are added, the base fluid becomes more thermally efficient. A hybrid nanofluid is a base fluid that contains two different nanoparticles. A ternary nanofluid is created by combining three different nanoparticles with a base fluid. When compared to simple and hybrid nanofluid, ternary hybrid nanofluid performs better in terms of thermal efficiency and fluid movement. Ternary nanofluids are employed in a variety of industries, including the medical sector, engineering detergent manufacture, automobile cooling, nuclear reactor cooling brake fluid, and military uses. Ramzan et al. [13] studied how a magnetic field over the stretched surface affected the two-dimensional movement of the Carreau-tri-hybrid nano-liquid about heat radiation and heat source/sink. The movement of an electroconductive incompressible tri-hybrid nano-liquid with heat transfer in incorporating metal tiny particles along a stretching cylinder with magnetic induction effects is investigated by Alharbi et al. [14]. With a new non-Fourier heat flux model, the influence of internal heat generation in the exponential form on tri-hybrid nanofluid movement was studied by Sarada et al. [15]. Sahoo and Kumar [16] studied how temperature and nanoparticle concentrations affected the dynamic viscosity of a water-based tri-hybrid nano-liquid. Maranna et al. [17] studied how heat radiation and the Navier–Stokes equation affected the circulation of Walter's B tri-hybrid nano liquids and second-grade nano liquids via a permeable shrinking plane surface.

Being a fundamental feature of matter dependent on its temperature, thermal radiation is one of the three fundamental types of heat transport (conduction, convection, and radiation). Thermal radiation, whose properties depend on the temperature of the source material. Mahesh et al. [18] studied the influence of absorption/injection motion of Casson liquid and heat radiation on a permeable surface in the existence of a magnetic field. Mukhtar et al. [19] studied numerically the outcomes of a mathematical model for boundary layer motion caused by unsteady magnetohydrodynamics on a porous stretched surface Sreedevi and Sudarsana [20] studied the effect of thermal radiation on Williamson nanofluid motion over a wedge used by multi-walled carbon nanotube nanomaterials with kerosene as the base fluid. Zahid et al. [21] studied mass transfer and bioconvection, the nonlinear magnetohydrodynamic motion of nanofluids through an expanding sheet in the presence of a porous medium. Habib et al. [22] studied the importance of bioconvection and mass dissipation for magnetohydrodynamic micropolar Maxwell nano-liquid circulation across an extended sheet. Habib et al. [23] explored the influence of the magnetic transfer of heat and mass on the movement of micropolar liquid across a permeable stretching geometry with diluted homogenous dispersion of nanoparticles and gyrotactic microorganisms.

Mahabaleshwar et al. [24] studied the movement of a porous stretching/shrinking sheet over a three-dimensional incompressible viscoelastic fluid containing hybrid nano-liquids and chemical reaction rate. Khan et al. [25] examined a two-dimensional Casson fluid circulation through a contracting and stretching sheet that is dependent on mixed convection, convective state, and slip condition. Heat and mass transfer in nanofluid circulation across an extended sheet affected by

viscous dissipation, hydromagnetic, and chemical reactions were examined by Kameswaran et al. [26]. Bhattacharyya et al. [27] discovered the impact of partial slip on steady boundary layer stagnation-point movement of an incompressible liquid and the transmission of heat to a shrinking sheet. Fang et al. [28] examined the viscous motion across a shrinking surface using a 2nd-order slip movement model.

Aslani et al. [29] studied mass transpiration and slanting magnetohydrodynamic movement of a micropolar liquid through a porous Stretching/Shrinking sheet in combination with radiation. Yasir et al. [30] explored the impact of mass transpiration on the rotational motion of a radiative hybrid nanofluid caused by a shrinking surface with a non-uniform heat source/sink. Zahid et al. [31] studied nanofluid flow in a porous medium with mass transpiration and bioconvection during nonlinear magnetohydrodynamic movement across an extended sheet. Habib et al. [32] studied how the flow of micropolar liquid through a porous media stretching geometry with diluted consistent dispersion of nanoparticles and gyrotactic microorganisms would be affected by the magnetic impact of mass as well as heat transfer. Maranna et al. [33] examined how radiation and Marangoni convective boundary conditions affected the movement of nanofluids in a permeable media with a mass transpiration effect.

2. MATHEMATICAL FORMULATION AND SOLUTIONS

A non-Newtonian steady laminar flow of Ostwald–de Waele fluid across a surface with mass transpiration is evaluated and shown in Fig. 1 momentum elements are denoted by u along x axis and v along y axis. The boundary shrinks at the momentum $Uw\,(x) = -Bx$, where B is positive constant, and momentum of the mass transpiration denotes as $V_w\,(x)$. Ternary nanoparticles combined in pure water to obtain the thermal efficiency of the liquid.

The stress tensor of power-law fluid is stated as [2, 33]:

$$\xi_{xy} = \mu\,(\dot{\gamma})\,\dot{\gamma}. \tag{1}$$

Strain-rate's second invariant tensor denotes as $\dot{\gamma}$ and μ is constitutive viscosity and determined by power-law as [2]

$$\mu\,(\dot{\gamma}) = K\,|\dot{\gamma}|^{n-1}\,, \tag{2}$$

where n is denoted as non-Newtonian fluids degree, and if $n = 1$ called Newtonian rheology, $n < 1$ denotes shear-thinning pseudoplastic range, $n > 1$ is dilatants class, and K is denoted as consistency factor.

With the assumptions of boundary layer the shear tensor converted as [2, 33]:

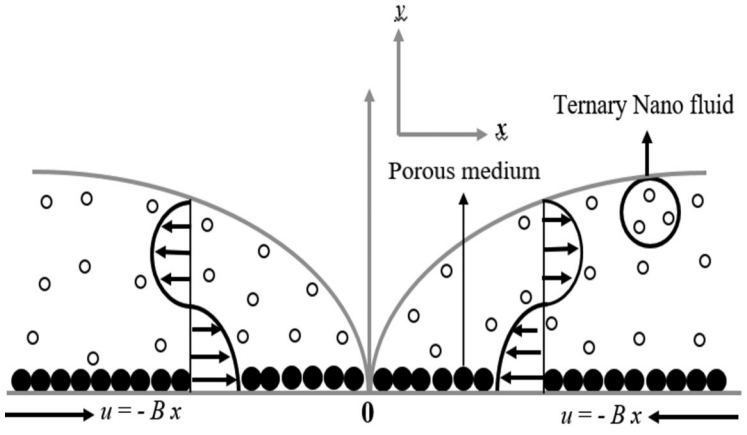

Fig. 1. Schematic representation of the fluid flow.

$$\xi_{xy} = K\left|\frac{\partial u}{\partial y}\right|^{n-1}\frac{\partial u}{\partial y}. \tag{3}$$

The governing equations of the problem are stated as [33]:

$$\frac{\partial u}{\partial x} + \frac{\partial v}{\partial y} = 0, \tag{4}$$

$$u\frac{\partial u}{\partial x} + v\frac{\partial u}{\partial y} = \frac{\mu_{eff}}{\rho_{tnf}}K\frac{\partial}{\partial y}\left(\frac{\partial u}{\partial y}\right)^{n} - \frac{\mu_{tnf}}{K^{*}\rho_{tnf}}u. \tag{5}$$

B.Cs are given as follows [33]

$$\left.\begin{aligned} &u = U_w(x) = -Bx,\ v = V_w(x),\ \text{at } y = 0,\\ &u = 0, \qquad\qquad\qquad\qquad \text{as } y \to \infty \end{aligned}\right\}. \tag{6}$$

Here u and v are velocity components along x and y axes respectively, denoting the Brinkman ratio, denote the density, the dynamic viscosity, K^{*} denotes the permeability coefficient.

The suitable similarity variables and stream function as follows

$$\left.\begin{aligned} &\psi(x,y) = \left(\frac{K/\nu_f}{B^{1-2n}}\right)^{\frac{1}{n+1}} x^{\frac{2n}{n+1}} f(\eta), \quad \eta = y\left(\frac{B^{2-n}}{K/\nu_f}\right)^{\frac{1}{n+1}} x^{\frac{1-n}{n+1}},\\ &u = \frac{\partial \psi}{\partial y} = Bx\, f_{\eta}(\eta),\\ &v = -\frac{\partial \psi}{\partial x} = -\frac{1}{1+n}\left(\frac{K/\nu_f}{B^{1-2n}}\right)^{\frac{1}{n+1}} x^{\frac{n-1}{n+1}}\left(2nf + (1-n)\,\eta f_{\eta}(\eta)\right) \end{aligned}\right\}, \tag{7}$$

using the above similarity variables the governing equations are calculated as follows

$$\Lambda n\left(f_{\eta\eta}(\eta)\right)^{n-1} f_{\eta\eta\eta}(\eta) - A_2\left[\left(f_{\eta}(\eta)\right)^{2} - \frac{2n}{n+1}f(\eta)\, f_{\eta\eta}(\eta)\right] - A_1 Da^{-1} = 0, \tag{8}$$

where Λ is Brinkman parameter, $A_1 = \frac{\mu_{tnf}}{\mu_f}$ and $A_2 = \frac{\rho_{tnf}}{\rho_f}$ are constants, $Da^{-1} = \frac{\mu_f}{\rho_f K^{*} B}$ is inverse Darcy parameter.

The modified B.Cs are given as follows [2, 33]

$$f'(0) = -1, \quad f'(\infty) = 0, \quad f(0) = S, \tag{9}$$

where S denotes the mass transpiration at the wall, $S > 0$ denotes the mass suction, and $S < 0$ denotes mass injection.

Mass transfer $V_w(x)$ calculated as [2]

$$V_w(x) = -\frac{2n}{n+1}\left(\frac{K/\nu_f}{B^{1-2n}}\right)^{\frac{1}{n+1}} x^{\frac{n-1}{n+1}} S. \tag{10}$$

In the current analysis, obtaining a closed-form solution for some special cases, corresponds to linear rheology $n = 1$, assuming the exact solution for Newtonian flow as follows [2, 33]

$$f(\eta) = \beta + \frac{1}{\beta}\exp(-\beta\eta). \tag{11}$$

Here $\beta = f(\infty) = f''(0)$, the BCs have dual solutions for β when $S > 2$. β has a unique solution for $S = 2$, and has no solution for $0 \leq S < 2$, adding $n = 1$ into Eq. (8) which gives

$$\Lambda f_{\eta\eta\eta}(\eta) - A_2\left[(f_\eta(\eta))^2 - f(\eta) f_{\eta\eta}(\eta)\right] - A_1 Da^{-1} = 0. \tag{12}$$

Suppose flow past a non-permeable surface Eq. (12) becomes

$$\Lambda f_{\eta\eta\eta}(\eta) - A_2\left[(f_\eta(\eta))^2 - f(\eta) f_{\eta\eta}(\eta)\right] = 0. \tag{13}$$

The solution for Eq. (11) calculated as

$$f(\eta) = \frac{6}{\frac{A_2}{\Lambda}\eta + \sqrt{6\frac{A_2}{\Lambda}}}, \tag{14}$$

which reduces mass transpiration $S = \sqrt{\frac{6\Lambda}{A_2}}$. The inclusion of the power function makes it difficult to reduce mass transpiration in Eq. (16). Referring to Fang [28], the solution for Eq. (8) is given as

$$f(\eta) = \frac{k}{(\eta + m)^\beta}. \tag{15}$$

To satisfy the B.Cs $f(\infty) = 0$, the choice β must be non-negative. By using Eqs. (15) and (8), the resulting equations become

$$\begin{aligned} n\left[k\beta(\beta+1)\right]^{n-1}\left[-(\beta+1)(\beta+2)(\eta+m)^{-(\beta-2)(n-1)-\beta-3}\right] - \frac{A_2}{\Lambda}k\beta(\eta+m)^{-2\beta-2} \\ + \frac{A_2}{\Lambda}\frac{2n}{n+1}k(\beta+1)(\eta+m)^{-2\beta-2} + \frac{A_1 Da^{-1}}{\Lambda}(\eta+m)^{-\beta-1} = 0. \end{aligned} \tag{16}$$

To solve this problem, Eq. (16) calculated as

$$-n\left[k\beta(\beta+1)^{n-1}\right](\beta+1)(\beta+2) = \frac{A_2}{\Lambda}k\beta - \frac{A_2}{\Lambda}\frac{2n}{n+1}k(\beta+1) - \frac{A_1 Da^{-1}}{\Lambda}(\eta+m)^{\beta+1}. \tag{17}$$

By solving both equations (16) via (17) we get

$$(\beta+2)(n-1) + (\beta+3) = 2(\beta+1). \tag{18}$$

Simplify the above equation and give β value as

$$\beta = \frac{2n-1}{2-n}. \tag{19}$$

Positivity parameter n induces range lies between $\frac{1}{2} < n < 2$. Taking $\eta = 0$ in Eq. (17), the solution of k is gained as

$$k = \left(\frac{(2n-1)(n+1)}{(2-n)^2}\right)^{\frac{1-n}{n-2}} \left[\frac{(2-n)\left(\frac{A_2}{\Lambda} + (-1+2n)\frac{A_1 Da^{-1}}{\Lambda}\right)}{3n(n+1)}\right]^{\frac{1}{n-2}} \tag{20}$$

for $\eta \neq 0$ still we can calculate k using Eq. (17) but there is no analytical procedure for calculating $\psi(x,y)$, by using B.Cs and assuming the solution of the velocity equation obtain the following results

$$f(0) = km^{-\beta} = S, \quad f_\eta(\eta) = -k\beta m^{-\beta-1} = -1, \quad f_{\eta\eta}(0) = k\beta(\beta+1)m^{-\beta-2} = (\beta+1)m^{-1}, \tag{21}$$

by using the above equation we derive the following result

$$S = k^{1/\beta+1}\beta^{-\beta/\beta+1} = \left(\frac{2n-1}{2-n}\right)^{-(2n-1/n+1)} \left(\frac{(2n-1)(n+1)}{(2-n)^2}\right)^{n-1/n+1}$$

$$\times \left(\frac{(2-n)\left(\frac{A_2}{\Lambda} + (-1+2n)\frac{A_1 Da^{-1}}{\Lambda}\right)}{3n(n+1)}\right)^{-1(1/n+1)}, \tag{22}$$

we can calculate m as follows

$$m = S\beta \quad = \left(\frac{2n-1}{2-n}\right)^{(2-n/n+1)} \left(\frac{(2n-1)(n+1)}{(2-n)^2}\right)^{n-1/n+1}$$

$$\times \left(\frac{(2-n)\left(\frac{A_2}{\Lambda} + (-1+2n)\frac{A_1 Da^{-1}}{\Lambda}\right)}{3n(n+1)}\right)^{-(1/n+1)}. \tag{23}$$

Similarly, $f_{\eta\eta}(0)$ can be derived as

$$f_{\eta\eta}(0) = \frac{\beta+1}{m} = \frac{n+1}{2-n}\left(\frac{(2n-1)(n+1)}{(2-n)^2}\right)^{1-n/1+n}$$

$$\times \left(\frac{(2-n)\left(\frac{A_2}{\Lambda} + (-1+2n)\frac{A_1 Da^{-1}}{\Lambda}\right)}{3n(n+1)}\right)^{(1/n+1)} \left(\frac{2n-1}{2-n}\right)^{n-2/n+1}, \tag{24}$$

where $f_{\eta\eta}(0) > 0$ denotes the upper branch and $f_{\eta\eta}(0) < 0$ denotes the lower branch.

Via Eq. (15) $f(\eta)$ and $f_\eta(\eta)$ can be calculated as follows

$$f(\eta) = \left(\frac{(2n-1)(n+1)}{(2-n)^2}\right)^{1-n/n-2} \left(\frac{(2-n)\left(\frac{A_2}{\Lambda} + (-1+2n)\frac{A_1 Da^{-1}}{\Lambda}\right)}{3n(n+1)}\right)^{1/n-2}$$

$$\times \left\{\eta + \left(\frac{(2n-1)\left(\frac{A_2}{\Lambda} + (-1+2n)\frac{A_1 Da^{-1}}{\Lambda}\right)}{3n(n+1)}\right)^{-1/n+1} \left(\frac{(2n-1)(n+1)}{(2-n)^2}\right)^{n-1/n+1}\right.$$

$$\times \left(\frac{2n-1}{2-n}\right)^{2-n/n+1}\Bigg\}^{-(2n-1/2-n)}, \tag{25}$$

$$f_\eta(\eta) = -\left(\frac{2n-1}{2-n}\right)\left(\frac{(2n-1)(n+1)}{(2-n)^2}\right)^{1-n/n-2}\left(\frac{(2-n)\left(\frac{A_2}{\Lambda}+(-1+2n)\frac{A_1 Da^{-1}}{\Lambda}\right)}{3n(n+1)}\right)^{1/n-2}$$

$$\times\left(\eta+\left(\frac{(2-n)\left(\frac{A_2}{\Lambda}+(-1+2n)\frac{A_1 Da^{-1}}{\Lambda}\right)}{3n(n+1)}\right)^{-1/n+1}\left(\frac{(2n-1)(n+1)}{(2-n)^2}\right)^{n-1/n+1}\right.$$

$$\left.\times\left(\frac{2n-1}{2-n}\right)^{2-n/n+1}\right)^{-(n+1/2-n)}. \tag{26}$$

Select $K=\nu_f=B=1$, and streamline flow patterns described by the stream function given as,

$$\psi(x,y) = x^{2n/n+1}\left(\frac{(2-n)\left(\frac{A_2}{\Lambda}+(-1+2n)\frac{A_1 Da^{-1}}{\Lambda}\right)}{3n(n+1)}\right)^{1/n-2}\left(\frac{(2n-1)(n+1)}{(2-n)^2}\right)^{1-n/n-2}$$

$$\times\left\{yx^{1-n/n+1}+\left(\frac{(2-n)\left(\frac{A_2}{\Lambda}+(-1+2n)\frac{A_1 Da^{-1}}{\Lambda}\right)}{3n(n+1)}\right)^{-1/n+1}\left(\frac{(2n-1)(n+1)}{(2-n)^2}\right)^{n-1/n+1}\right.$$

$$\left.\times\left(\frac{2n-1}{2-n}\right)^{2-n/n+1}\right\}^{2n-1/2-n}. \tag{27}$$

When $n=1$, the algebraic form of Eq. (27) calculated as

$$\psi(x,y) = x\frac{6}{\left(\frac{A_2+A_1 Da^{-1}}{\Lambda}\right)\eta+\sqrt{6\left(\frac{A_2+A_1 Da^{-1}}{\Lambda}\right)}}. \tag{28}$$

For S tends to infinity, from Eq. (11) assumed, $f(\eta)=S+\delta(\lambda)/S$, where $\lambda=\eta S$. Then the velocity equation becomes

$$n(S\delta_{\lambda\lambda})^{n-1}S^2\delta_{\lambda\lambda\lambda}-\frac{A_2}{\Lambda}\left(\delta_\lambda^2-\frac{2n}{n+1}\left(S+\frac{\delta}{S}\right)S\delta_{\lambda\lambda}\right)-\frac{A_1}{\Lambda}Da^{-1}\delta_\lambda=0. \tag{29}$$

Here, the variable λ denotes the total differentiation concerning λ. Put $n=1$ and let $S\to\infty$ in Eq. (29) becomes

$$\delta_{\lambda\lambda\lambda}+\frac{A_2}{\Lambda}\delta_{\lambda\lambda}=0. \tag{30}$$

Associated B.Cs reduce to

$$\delta(0)=0,\quad \delta_\lambda(0)=-1,\quad \delta_\lambda(\infty)=0. \tag{31}$$

The asymptotic values of the momentum equation are calculated as

$$\delta(\lambda) = \exp(-\lambda) - 1, \quad \delta_\lambda(\lambda) = -\exp(-\lambda). \tag{32}$$

Also letting $S \to \infty$ for $n < 1$, $n > 1$ in Eq. (29) as follows

$$\delta_{\lambda\lambda} = 0, \tag{33}$$

$$(\delta_{\lambda\lambda})^{n-1}\, \delta_{\lambda\lambda\lambda} = 0. \tag{34}$$

Asymptotic suction momentum profiles of the two cases are the same and given as

$$\delta(\lambda) = -\lambda, \;\; \delta_\lambda(\lambda) = -1. \tag{35}$$

3. RESULTS AND DISCUSSION

The study focuses on a consistent, smooth flow of non-Newtonian Ostwald–de Waele fluid on a contracting surface with mass transpiration, to improve the thermal efficiency of the fluid, ternary nanoparticles are combined with pure water, and the governing PDEs are converted to nonlinear ODEs via similarity variables and solved analytically. The article includes closed-form algebraic solutions and graphical flow dynamics analysis, dependent on Darcy number, volume fraction, and mass transpiration. Table 1 represents the thermo-physical properties of ternary nano particles and base fluid.

According to past studies, the ternary nanofluid quantity viscosity is defined as

$$\mu_{thnf} = \frac{1}{(1-\varphi_{TiO_2})^{2.5}\,(1-\varphi_{CoFe_2O_4})^{2.5}\,(1-\varphi_{MgO})^{2.5}}.$$

Considering the structure of nanoparticle effects the density in ternary nanofluid is subsequently defined as

$$\frac{\rho_{thnf}}{\rho_f} = (1-\varphi_{\mathrm{TiO_2}})\Bigg\{(1-\varphi_{\mathrm{CoFe_2O_4}})\left[(1-\varphi_{\mathrm{MgO}}) + \varphi_{\mathrm{MgO}}\frac{\rho_{\mathrm{MgO}}}{\rho_f}\right] + \varphi_{\mathrm{CoFe_2O_4}}\frac{\rho_{\mathrm{CoFe_2O_4}}}{\rho_f}\Bigg\} + \varphi_{\mathrm{TiO_2}}\frac{\rho_{\mathrm{TiO_2}}}{\rho_f}.$$

Figures 2–5 portray the graphs of k, m, S, and $f_{\eta\eta}(0)$ over n where solid lines show the result of Fang's analysis and dotted lines shows the current analysis. We obtain Fang's result by setting $Da^{-1} = 0$, $\varphi = 0$ to our result, since no permeable media and no nanoparticles are added in Fong's work. Saw that the values of S and $f_{\eta\eta}(0)$ decay monotonically with the upsurge of n as portrayed Figs. 4 and 5; but this influence is shows different phinamena, both are upsurging with the rise of n as shown in Figs. 2 and 3. And n upsurges beyond certain range, the choices rise continously is depicted in Fig. 2. saw that the more choices of decay for values of k, m, and S; and only values $f_{\eta\eta}(0)$ is higher.

Figure 6 portrays the effect of various choices, solid lines show the analysis of Fang and the dotted plots show the current analysis. saw that $f(\eta)$ decreases for higher choices of n. Figures 7–9

Table 1. Thermo-physical properties of ternary nanoparticles and base fluid

Properties	H_2O	Titanium dioxide (TiO_2)	Cobalt ferrite ($CoFe_2O_4$)	Magnesium oxide (MgO)
ρ (kgm^{-3})	997.1	4250	4907	3560

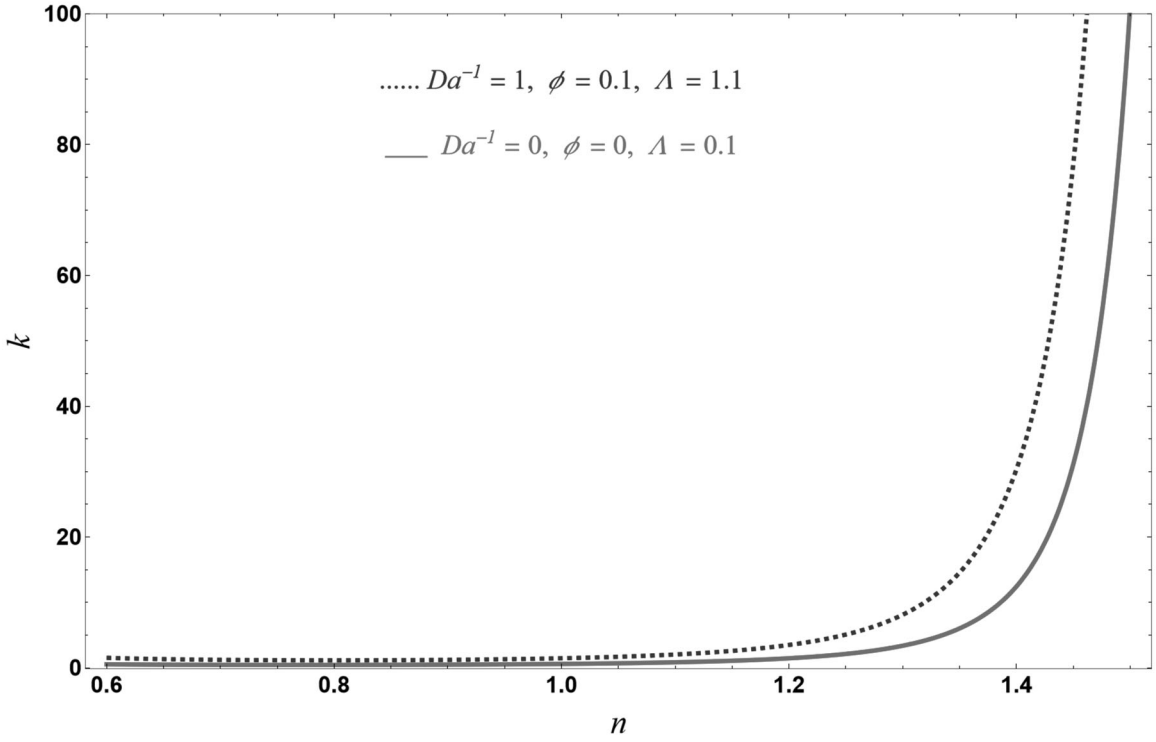

Fig. 2. Influence of n on consistency parameter.

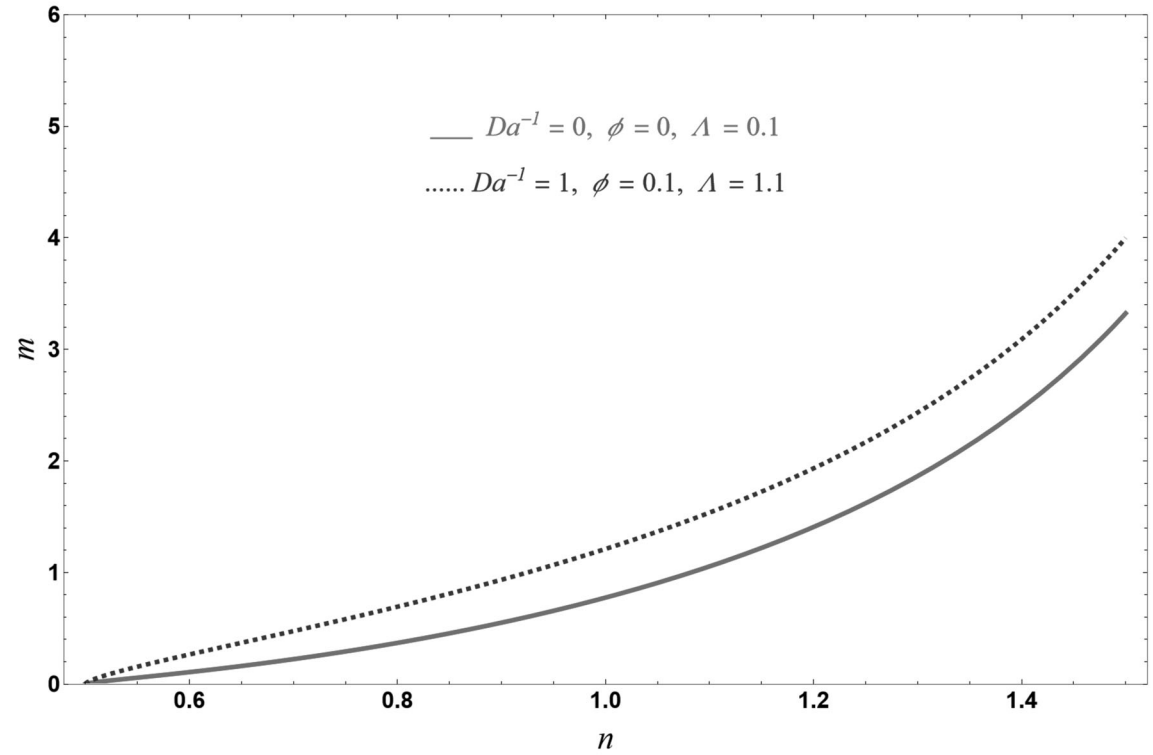

Fig. 3. Influence of n on m.

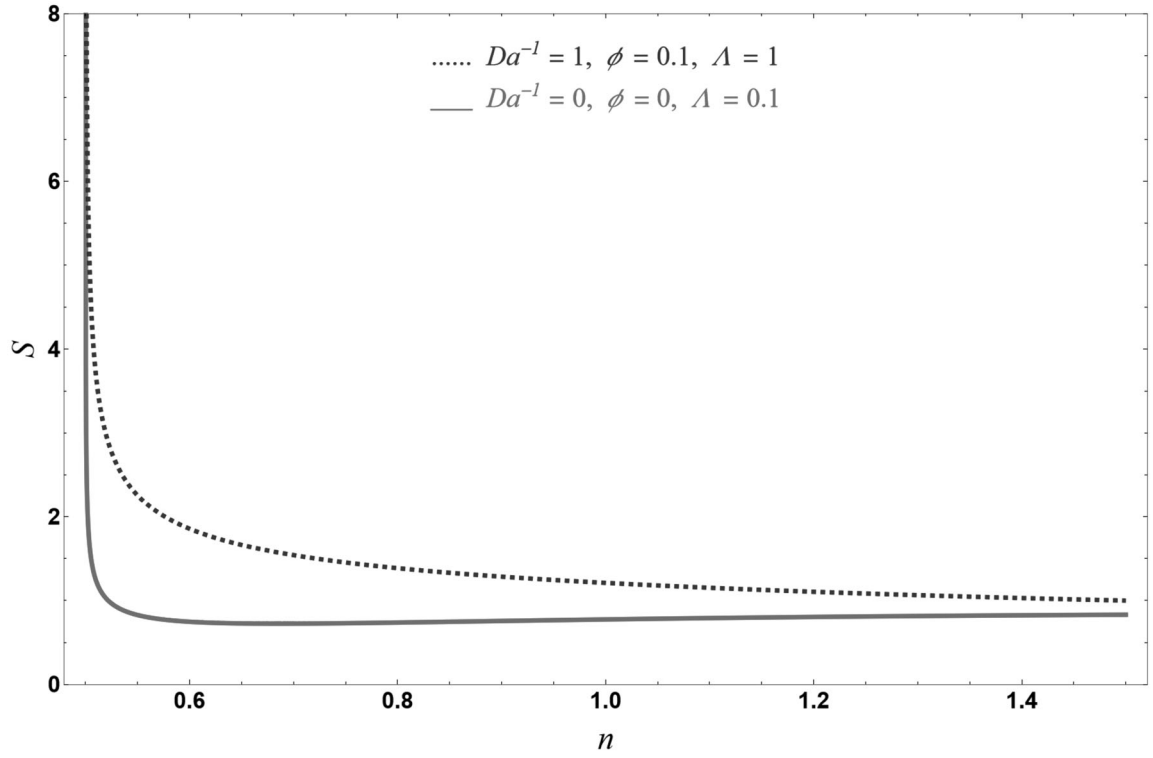

Fig. 4. Influence on Mass transpiration.

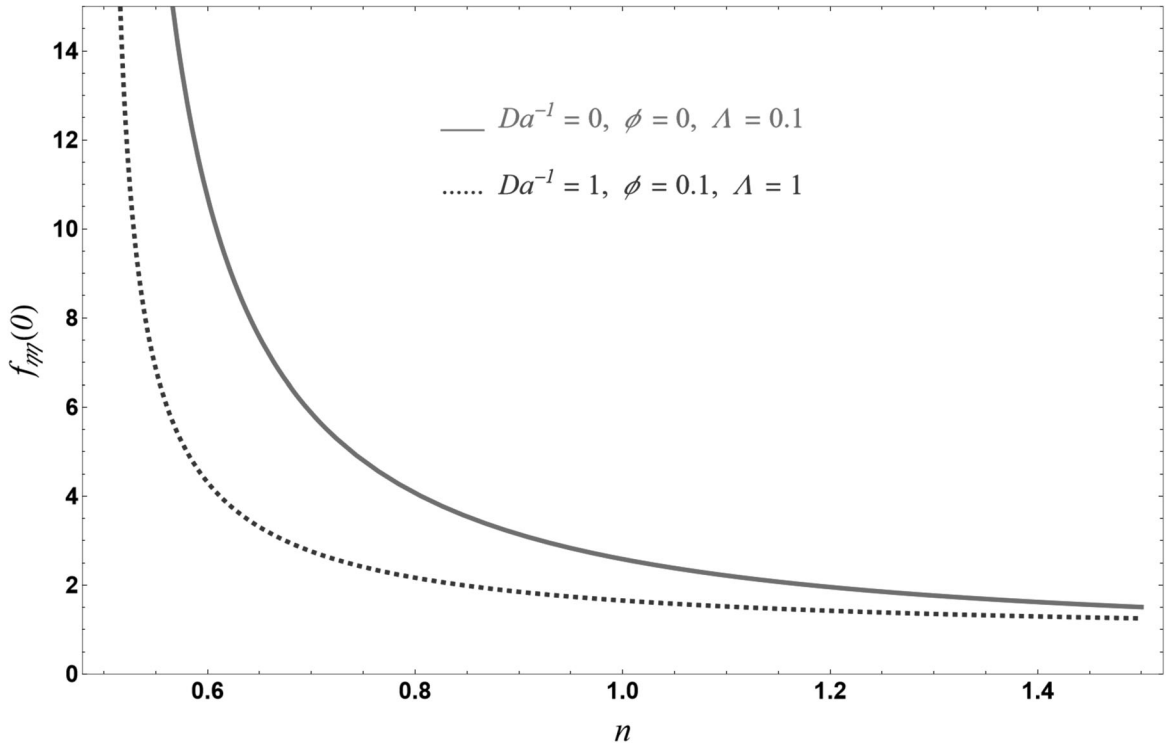

Fig. 5. Influence n on $f_{\eta\eta}(0)$.

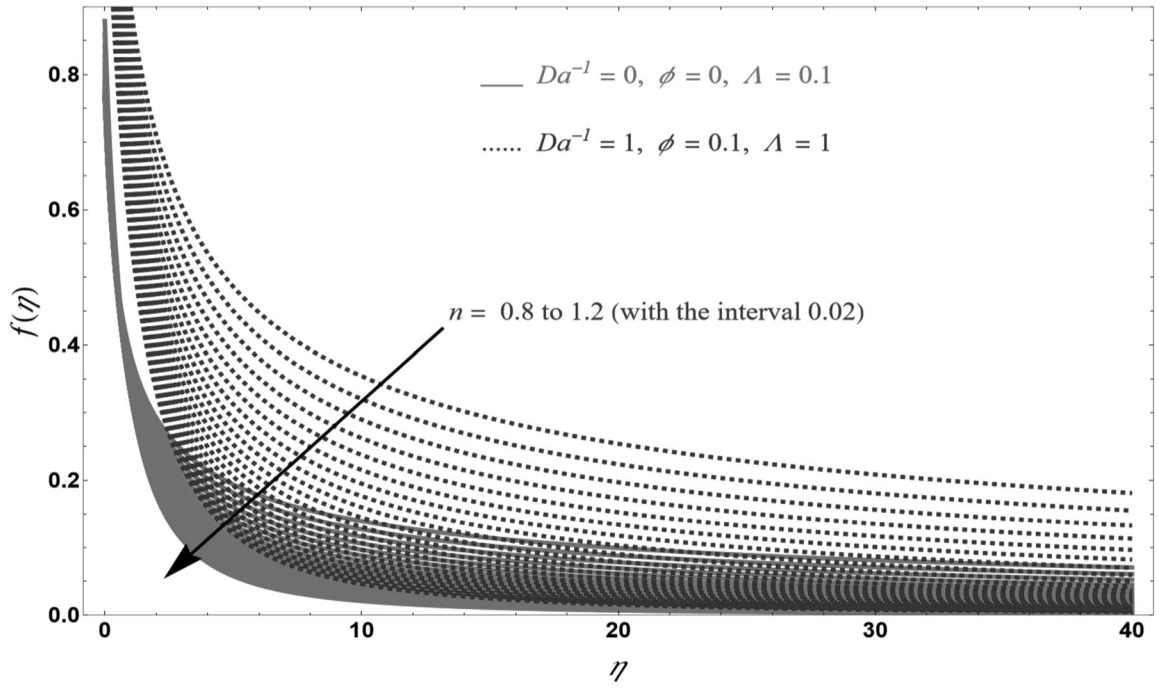

Fig. 6. $f(\eta)$ versus η for different values of n.

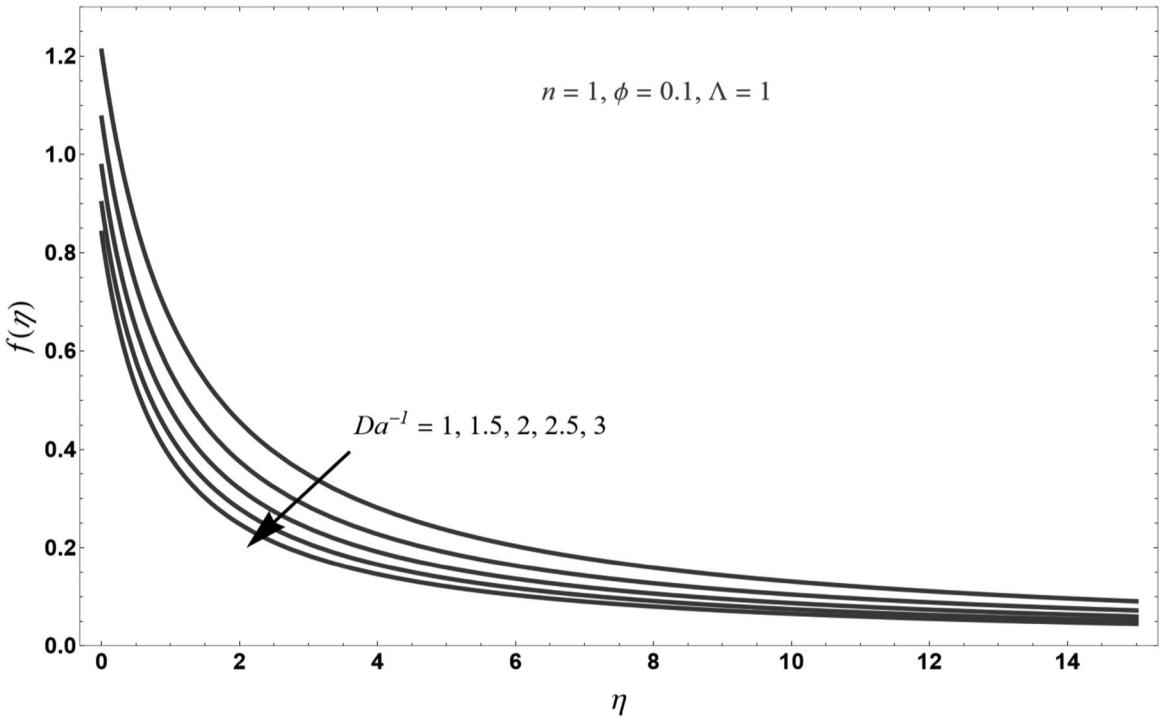

Fig. 7. $f(\eta)$ versus η for various choices with fixed values of $n = 1$, $\Lambda = 1$, and $\varphi = 0.1$.

portrays the impact of η by changing the values the Da^{-1}, Λ, and ϕ. It is shown that $f(\eta)$ is a monotonically decays by upsurging of Da^{-1} and ϕ, but the decaying of Λ upsurges $f(\eta)$, and upsurging function of $f(\eta)$ for different choices of n as saw in Fig. 10 and greater values of n, Da^{-1} and provides higher $f(\eta)$.

Figure 11 indicates the influence of the η on the non-dimensional velocity. The momentum decays with the choices of n upsurge, volume fraction rising decays the vertical velocity.

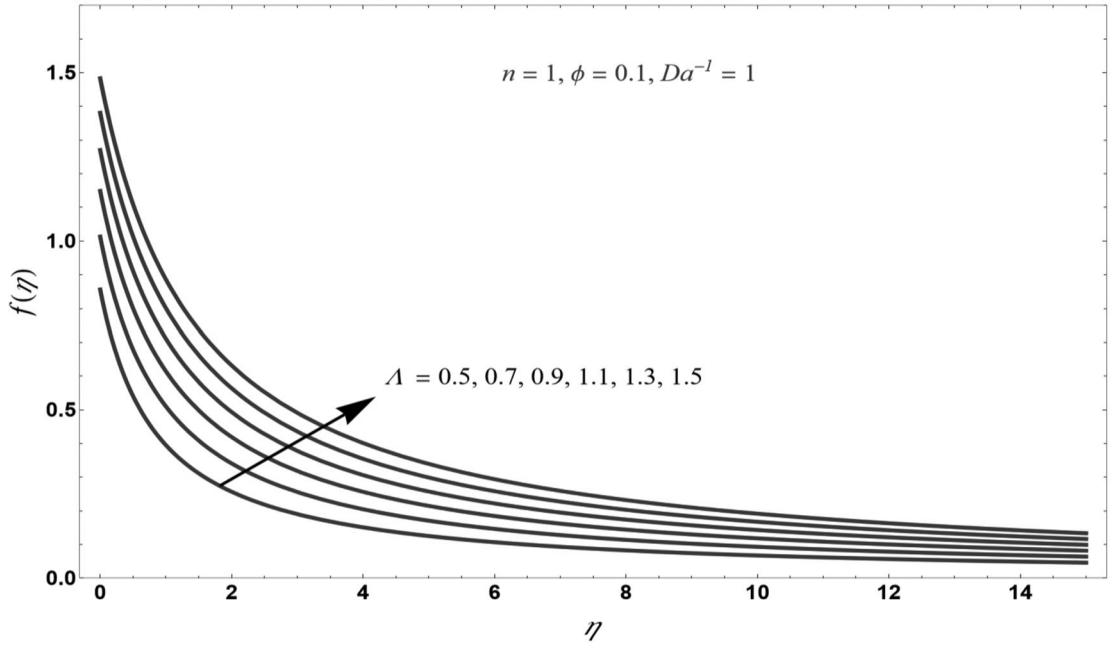

Fig. 8. $f(\eta)$ versus η for various choices with fixed terms $n = 1$, $Da^{-1} = 1$, and $\varphi = 0.1$.

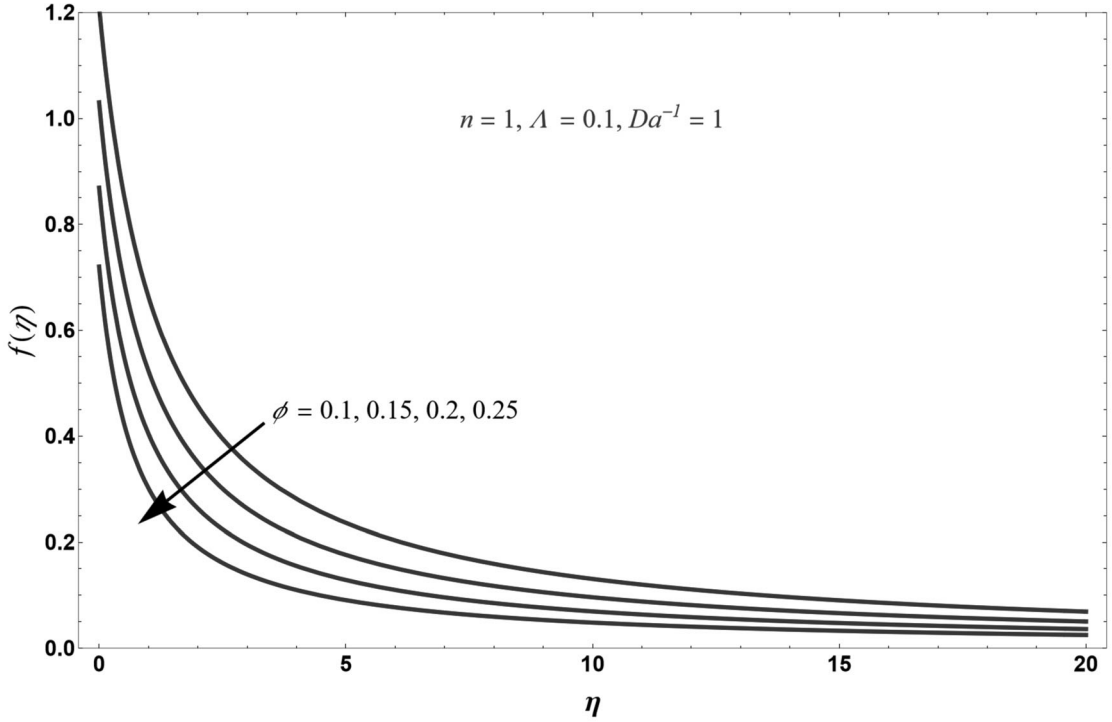

Fig. 9. $f(\eta)$ versus η for various choices with fixed terms $n = 1$, $Da^{-1} = 1$, and $\Lambda = 1$.

Figures 12–14 portrays influence of $f_\eta(\eta)$ on η for different choice of Da^{-1}, φ, and Λ where solid lines are analysis of Fang and dashed lines shows the current analysis. Tangential velocity $f_\eta(\eta)$ decreases with increases and the $f_\eta(\eta)$ is always in the non-positive direction, increasing the volume fraction decreases the tangential velocity profile, and increasing the Brinkman parameter increases the tangential velocity $f_\eta(\eta)$. Figure 15 portrays the impact of Da^{-1} on $[f_{\eta\eta}(0)]^n$. These plots shows dual nature which are gained by Eq. (10). For an higher branch of the solution $[f_{\eta\eta}(0)]^n$ rises

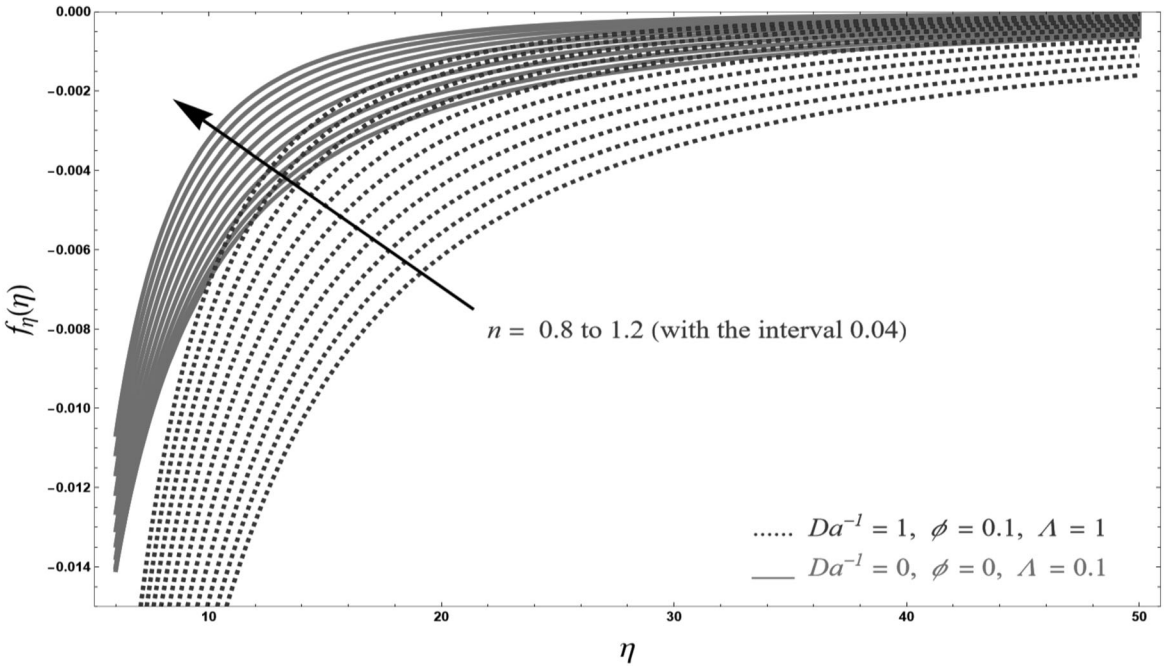

Fig. 10. Influence of $f_\eta(\eta)$ for various values of n.

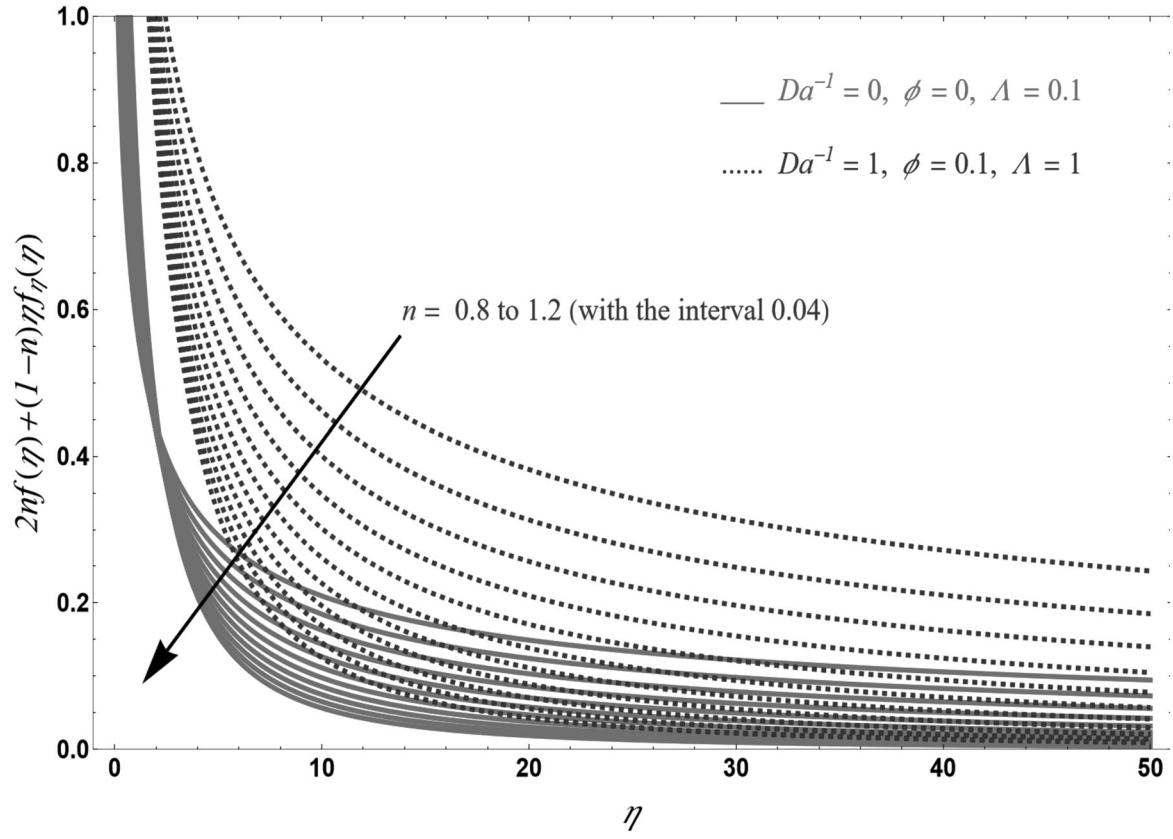

Fig. 11. Vertical velocity profile versus η for value of n.

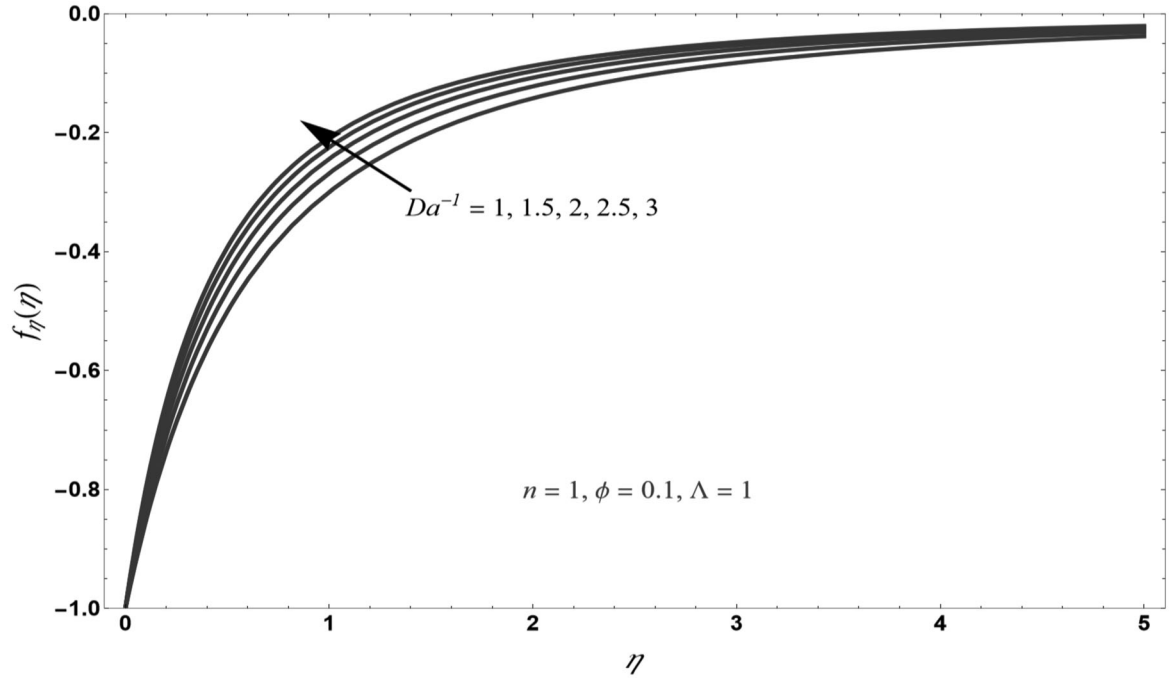

Fig. 12. Influence on various values of Da^{-1} with fixed parameter $\Lambda = 1$, $\phi = 0.1$, and $n = 1$.

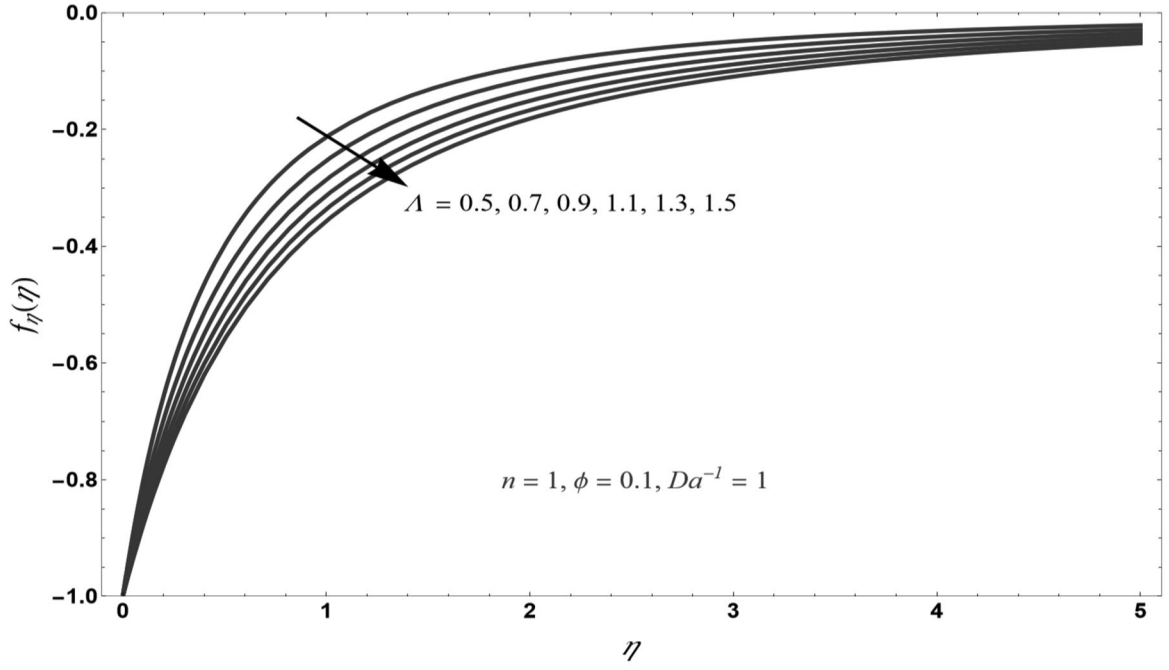

Fig. 13. Impact of $f_\eta(\eta)$ on η for various choices of $\Lambda$with fixed parameter $Da^{-1} = 1$, $\phi = 0.1$, and $n = 1$.

for upsurging choices of Da^{-1} but it decreases for upsurging of n, but shows reverse phenomena for lower solutions.

To study the flow field shown by the algebraic solution and the stream line graphs are depicted in Fig. 16. for different values of n. Here solid lines show the analysis of Fang and the dashed lines shows current analysis. here upsurges from 0.6, to 1.4, the streamlines' plots moves upward and become straight line at some point and moves downward.

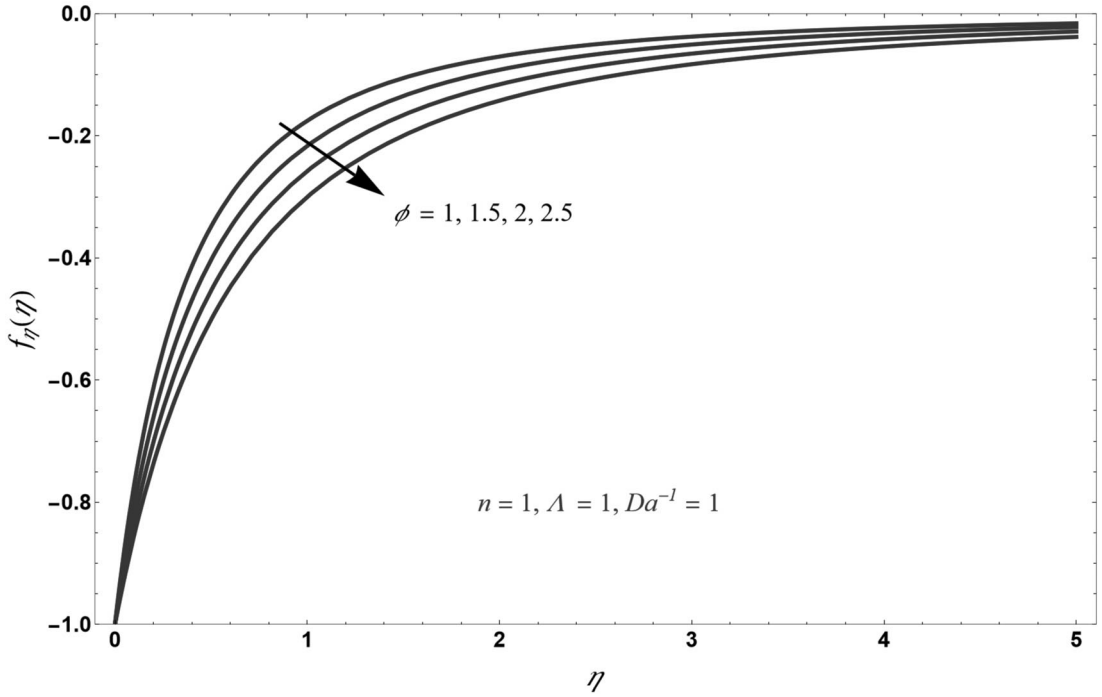

Fig. 14. Influence of $f_\eta(\eta)$ on η for various values of φ.

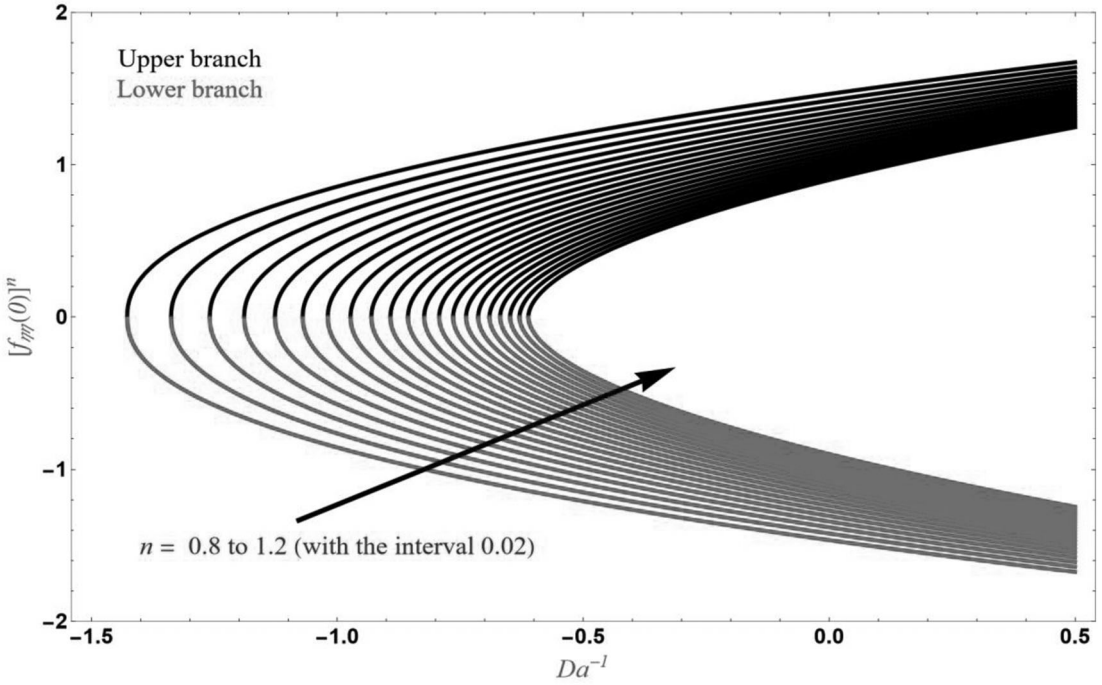

Fig. 15. $[f_{\eta\eta}(0)]^n$ versus the various values of n.

4. CONCLUSIONS

The present analysis investigates the Ostwald–de Waele fluid flow over a permeable shrinking surface with S, ternary nanoparticles dispersed in pure water. The solutions are exactly solved with several parameters and the influence of Ostwald–de Waele fluid on profiles of momentum and $[f_{\eta\eta}(0)]^n$ is shown by graphical analysis. Current analysis obtains closed-form analytic solutions that

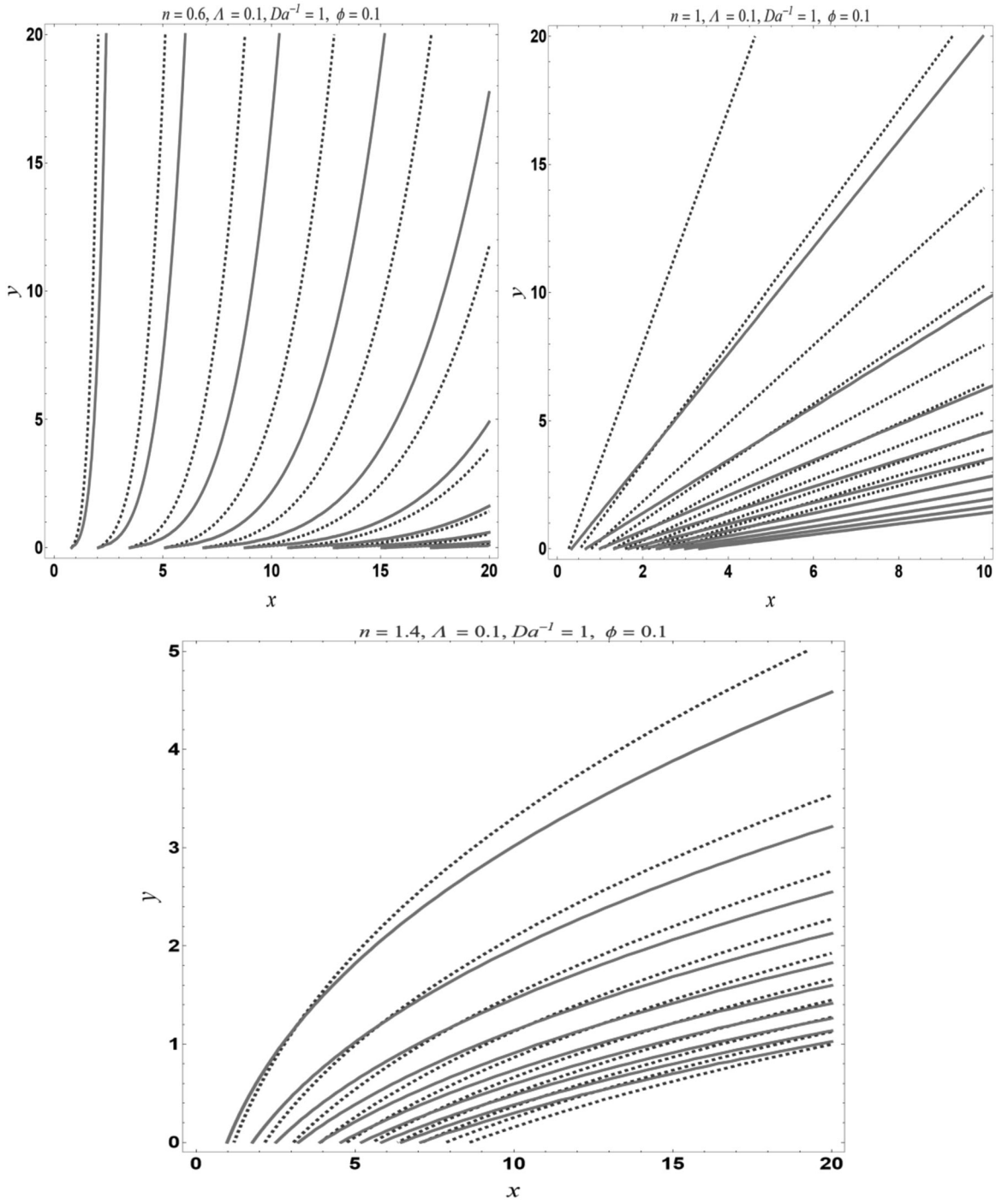

Fig. 16. Streamlines for different values of n.

are evaluated for algebraic solutions. Quantitative exact solutions give an necessary understanding of the fluid flow for Ostwald–de Waele nanofluids. By current analysis concludes as follows:

- $f(\eta)$ and decays with increases in the presence of Da^{-1}.
- $f_\eta(\eta)$ always occurred in a negative direction.
- S decays by upsurging the values of n.
- Momentum profile upsurges by raising the values of n.
- Dual solutions obtain for the shrinking surface.

- Skin friction upsurges with rising the choices of inverse Darcy number.
- Current analysis encourages the researchers to study boundary layer problems with Ostwald–de Waele fluid under different boundary conditions.

NOTATIONS

A_1 and A_2—constants [–]

B and C—constants [–]

K—consistency coefficient [–]

f—transverse velocity [m^2/s]

k and m—constants [–]

f_η—tangential velocity [m^2/s]

H_2O—water [–]

n—power-law index [–]

S—mass transfer parameter [m]

U_w—shrinking velocity [m^2/s]

$V_w(x)$—mass transfer velocity (ms^{-1})

u and v—velocity components (ms^{-1})

(x, y)—Cartesian coordinates [m]

Greek Symbols

β—solution domain [–]

η—similarity variable [–]

ρ—density (Kgm^{-3})

ϕ—volume fraction [–]

ψ—stream function [–]

ξ_{xy}—shear stress tensor [–]

Abbreviations

MHD—magnetohydrodynamics [–]

ODE—ordinary differential equations [–]

PDE—partial differential equations [–]

FUNDING

LMP acknowledges financial support from ANID through Convocatoria Nacional Subvencón a Instalacón en la Academia Convocatoria año. 2021, grant SA77210040.

CONFLICT OF INTEREST

The authors of this work declare that they have no conflicts of interest.

REFERENCES

1. Pang, B., Wang, S., and Lu, H., A Modified Drag Model for Power-Law Fluid-Particle Flow Used in Computational Fluid Dynamics Simulation, *Adv. Powder Technol.*, 2021, vol. 32, no. 4, pp. 1207–1218; DOI:10.1016/j.apt.2021.02.023
2. Mahabaleshwar, U.S., Vishalakshi, A.B., Huang, H.-N., and Öztop, H.F., An Effects of Mass Transpiration and Inclined MHD on Nano Boundary Layer of an Ostwald–de Waele Fluid Due to a Shrinking Boundary, *J. Magn. Magn. Mater.*, 2023, vol. 586, p. 171222; DOI:10.1016/j.jmmm.2023.171222
3. Elfeshawey, A.S. and Waheed, S.E., Effect of Viscous Dissipation and Thermal Radiation on MHD Flow and Heat Transfer for a Power-Law Fluid with Variable Fluid Properties over a Permeable Stretching Sheet, *Waves Random Complex Media*, 2022, pp. 1–15; DOI:10.1080/ 17455030.2022.2053610
4. Hussain, S. and Öztop, H.F., Impact of Inclined Magnetic Field and Power Law Fluid on Double-Diffusive Mixed Convection in the Lid-Driven Curvilinear Cavity, *Int. Comm. Heat Mass Transfer*, 2021, vol. 127, p. 105549; DOI:10.1016/j.icheatmasstransfer.2021.105549
5. Hu, X., Lin, J., Guo, Y., and Ku, X., Motion and Equilibrium Position of Elliptical and Rectangular Particles in a Channel Flow of a Power-Law Fluid, *Powder Technol.*, 2021, vol. 377, pp. 585–596; DOI:10.1016/j.powtec.2020.09.028
6. Usman, M., Lin, P., and Ghaffari, A., Steady Flow and Heat Transfer of the Power-Law Fluid between Two Stretchable Rotating Disks with Non-Uniform Heat Source/Sink, *J. Therm. An. Calorim.*, 2021, vol. 146, no. 4, pp. 1735–1749; DOI:10.1007/s10973-020-10142-x
7. Yadav, D., Chu, Y.M., and Li, Z., Examination of the Nanofluid Convective Instability of Vertical Constant through Flow in a Porous Medium Layer with Variable Gravity, *Appl. Nanosci.*, 2023, vol. 13, no. 1, pp. 353–366; DOI:10.1007/s13204-021-01700-2
8. Wahid, N.S., Arifin, N.M., Khashi'ie, N.S., and Pop, I., Marangoni Hybrid Nanofluid Flow over a Permeable Infinite Disk Embedded in a Porous Medium, *Int. Comm. Heat Mass Transfer*, 2021, vol. 126, p. 105421; DOI:10.1016/j.icheatmasstransfer.2021.105421
9. Waqas, H., Farooq, U., Khan, S.A., Alshehri, H.M., and Goodarzi, M., Numerical Analysis of Dual Variable of Conductivity in Bioconvection Flow of Carreau–Yasuda Nanofluid Containing Gyrotactic Motile Microorganisms over a Porous Medium, *J. Therm. An. Calorim.*, 2021, vol. 145, no. 4, pp. 2033–2044; DOI:10.1007/s10973-021-10859-3
10. Abd-Alla, A.M., Thabet, E.N., and Bayones, F.S., Numerical Solution for MHD Peristaltic Transport in an Inclined Nanofluid Symmetric Channel with Porous Medium, *Sci. Rep.*, 2022, vol. 12, no. 1, Art. no. 1; DOI:10.1038/s41598-022-07193-5
11. Eid, M.R. and Nafe, M.A., Thermal Conductivity Variation and Heat Generation Effects on Magneto-Hybrid Nanofluid Flow in a Porous Medium with Slip Condition, *Waves Random Complex Media*, 2022, vol. 32, no. 3, pp. 1103–1127; DOI:10.1080/17455030.2020.1810365
12. Reddy, Y.D., Mebarek-Oudina, F., Goud, B.S., and Ismail, A.I., Radiation, Velocity and Thermal Slips Effect toward MHD Boundary Layer Flow Through Heat and Mass Transport of Williamson Nanofluid with Porous Medium, *Arab. J. Sci. Eng.*, 2022, vol. 47, no. 12, pp. 16355–16369; DOI:10.1007/s13369-022-06825-2
13. Ramzan, M., Ali, F., Akkurt, N., Saeed, A., Kumam, P., and Galal, A.M., Computational Assessment of Carreau Ternary Hybrid Nanofluid Influenced by MHD Flow for Entropy Generation, *J. Magn. Magn. Mater.*, 2023, vol. 567, p. 170353; DOI:10.1016/j.jmmm.2023.170353
14. Alharbi, K.A.M., et al., Computational Valuation of Darcy Ternary-Hybrid Nanofluid Flow across an Extending Cylinder with Induction Effects, *Micromachines*, 2022, vol. 13, no. 4, Art. no. 4; DOI:10.3390/mi13040588
15. Sarada, K., et al., Impact of Exponential Form of Internal Heat Generation on Water-Based Ternary Hybrid Nanofluid Flow by Capitalizing Non-Fourier Heat Flux Model, *Case Stud Therm. Eng.*, 2022, vol. 38, p. 102332; DOI:10.1016/j.csite.2022.102332
16. Sahoo, R.R. and Kumar, V., Development of a New Correlation to Determine the Viscosity of Ternary Hybrid Nanofluid, *Int. Comm. Heat Mass Transfer*, 2020, vol. 111, p. 104451; DOI:10.1016/j.icheatmasstransfer.2019.104451
17. Maranna, T., Mahabaleshwar, U.S., Pérez, L.M., and Manca, O., Flow of Viscoelastic Ternary Nanofluid over a Shrinking Porous Medium with Heat Source/Sink and Radiation, *Therm. Sci. Eng. Prog.*, 2023, vol. 40, p. 101791; DOI:10.1016/j.tsep.2023.101791
18. Mahesh, R., Mahabaleshwar, U.S., Aly, E.H., and Manca, O., An Impact of CNTs on an MHD Casson Marangoni Boundary Layer Flow over a Porous Medium with Suction/Injection and Thermal Radiation, *Int. Comm. Heat Mass Transfer*, 2023, vol. 141, p. 106561; DOI:10.1016/j.icheatmasstransfer.2022.106561

19. Mukhtar, T., Jamshed, W., Aziz, A., and Al-Kouz, W., Computational Investigation of Heat Transfer in a Flow Subjected to Magnetohydrodynamic of Maxwell Nanofluid over a Stretched Flat Sheet with Thermal Radiation, *Numer. Meth. Part. Diff. Eq.*, 2023, vol. 39, no. 5, pp. 3499–3519; DOI:10.1002/num.22643
20. Sreedevi P. and Sudarsana Reddy, P., Heat and Mass Transfer Analysis of MWCNT-Kerosene Nanofluid Flow over a Wedge with Thermal Radiation, *Heat Transfer*, 2021, vol. 50, no. 1, pp. 10–33; DOI:10.1002/htj.21892
21. Zahid, M., Asjad, M.I., Hussain, S., and Akgül, A., Nonlinear Magnetohydrodynamic Flow of Nanofluids across a Porous Matrix over an Extending Sheet with Mass Transpiration and Bioconvection, *Heat Transfer*, 2021, vol. 50, no. 8, pp. 7588–7603; DOI:10.1002/htj.22244
22. Habib, D., Abdal, S., Ali, R., Baleanu, D., and Siddique, I., On Bioconvection and Mass Transpiration of Micropolar Nanofluid Dynamics due to an Extending Surface in Existence of Thermal Radiations, *Case Stud. Therm. Eng.*, 2021, vol. 27, p. 101239; DOI:10.1016/j.csite.2021.101239
23. Habib, D., Salamat, N., Ahsan, M., Abdal, S., Siddique, I., and Ali, B., Significance of Bioconvection and Mass Transpiration for MHD Micropolar Maxwell Nanofluid Flow over an Extending Sheet, *Waves Random Complex Media*, 2022, pp. 1–15; DOI:10.1080/17455030.2022.2088892
24. Mahabaleshwar, U.S., Anusha, T., Laroze, D., Said, N.M., and Sharifpur, M., An MHD Flow of Non-Newtonian Fluid Due to a Porous Stretching/Shrinking Sheet with Mass Transfer, *Sustainability*, 2022, vol. 14, no. 12, Art. no. 12; DOI:10.3390/su14127020
25. Khan, M.R., Elkotb, M.A., Matoog, R.T., Alshehri, N.A., and Abdelmohimen, M.A.H., Thermal Features and Heat Transfer Enhancement of a Casson Fluid across a Porous Stretching/Shrinking Sheet: Analysis of Dual Solutions, *Case Stud. Therm. Eng.*, 2021, vol. 28, p. 101594; DOI:10.1016/j.csite.2021.101594
26. Kameswaran, P.K., Narayana, M., Sibanda, P., and Murthy, P.V.S.N., Hydromagnetic Nanofluid Flow due to a Stretching or Shrinking Sheet with Viscous Dissipation and Chemical Reaction Effects, *Int. J. Heat Mass Transfer*, 2012, vol. 55, no. 25, pp. 7587–7595; DOI:10.1016/j.ijheatmasstransfer.2012.07.065
27. Bhattacharyya, K., Mukhopadhyay, S., and Layek, G.C., Slip Effects on Boundary Layer Stagnation-Point Flow and Heat Transfer towards a Shrinking Sheet, *Int. J. Heat Mass Transfer*, 2011, vol. 54, no. 1, pp. 308–313; DOI:10.1016/j.ijheatmasstransfer.2010.09.041
28. Fang, T., Yao, S., Zhang, J., and Aziz, A., Viscous Flow over a Shrinking Sheet with a Second Order Slip Flow Model, *Commun. Nonlin. Sci. Numer. Simul.*, 2010, vol. 15, no. 7, pp. 1831–1842; DOI:10.1016/j.cnsns.2009.07.017
29. Aslani, K.-E., Mahabaleshwar, U.S., Singh, J., and Sarris, I.E., Combined Effect of Radiation and Inclined MHD Flow of a Micropolar Fluid over a Porous Stretching/Shrinking Sheet with Mass Transpiration, *Int. J. Appl. Comput. Math.*, 2021, vol. 7, no. 3, p. 60; DOI:10.1007/s40819-021-00987-7
30. Yasir, M., Khan, M., Alqahtani, A.S., and Malik, M.Y., Mass Transpiration Effect on the Rotating Flow of Radiative Hybrid Nanofluid due to Shrinking Surface with Irregular Heat Source/Sink, *Case Stud. Therm. Eng.*, 2023, vol. 44, p. 102870; DOI:10.1016/j.csite.2023.102870
31. Zahid, M., Asjad, M.I., Hussain, S., and Akgül, A., Nonlinear Magnetohydrodynamic Flow of Nanofluids across a Porous Matrix over an Extending Sheet with Mass Transpiration and Bioconvection, *Heat Transfer*, 2021, vol. 50, no. 8, pp. 7588–7603; DOI:10.1002/htj.22244
32. Habib, D., Abdal, S., Ali, R., Baleanu, D., and Siddique, I., On Bioconvection and Mass Transpiration of Micropolar Nanofluid Dynamics due to an Extending Surface in Existence of Thermal Radiations, *Case Stud. Therm. Eng.*, 2021, vol. 27, p. 101239; DOI:10.1016/j.csite.2021.101239
33. Fang Tie-Gang, Tao Hua, and Zhong Yong-Fang, Non-Newtonian Power-Law Fluid Flow over a Shrinking Sheet, *Chin. Phys. Lett.*, 2012, vol. 29, no. 11, p. 114703; DOI:10.1088/0256-307X/29/11/114703